University of Huddersfield Repository

Hinks, J. A. and Donnelly, S. E.

Copper indium diselenide: crystallography and radiation-induced dislocation loops

Original Citation

This version is available at http://eprints.hud.ac.uk/16010/

http://eprints.hud.ac.uk/

Copper Indium Diselenide: Crystallography and Radiation Induced Dislocation Loops

J.A. Hinks* and S.E. Donnelly

*Corresponding author

Electron Microscopy and Materials Analysis (EMMA), T3/03 Technology Building, University of Huddersfield, Queensgate, Huddersfield, HD1 3DH, United Kingdom
E-mail: j.a.hinks@hud.ac.uk

Copper indium diselenide (CIS) is a prime candidate for the absorber layer in solar cells for use in extraterrestrial environments due to its good photovoltaic efficiency and ability to resist radiation damage. Whilst CIS-based devices have been tested extensively in the laboratory using electron and proton irradiation, there is still little understanding of the underlying mechanisms which give rise to its radiation hardness. In order to gain better insight into the response of CIS to displacing radiation, transmission electron microscope samples have been irradiated in situ with 400 keV Xe ions at the Intermediate Voltage Electron Microscope facility at Argonne National Laboratory, USA. At room temperature, dislocation loops were observed to form and to grow with increasing fluence. These loops have been investigated using $\boldsymbol{g.b}$ techniques and inside/outside contrast analysis. They were found to reside on {112} planes and to be interstitial in nature. The Burgers vector has been calculated to be $\boldsymbol{b}$ = 1/6 <221>. The compositional content of these interstitial loops was found to be indistinguishable from the surrounding matrix within the sensitivity of the techniques used. To facilitate this work, experimental electron-diffraction zone-axis pattern maps were produced and these are also presented along with analysis of the [100] zone-axis pattern.

Keywords: radiation damage; defect analysis; dislocation structures; crystallography; semiconductors; TEM; electron diffraction; ion irradiation; copper indium diselenide; $CuInSe_2$; CIS.

1   Introduction

Copper indium diselenide (CIS) is a chalcopyrite semiconductor with space group $I\bar{4}2d$. Along with its derivatives $(Cu(In,Ga)Se_2)$, CIS is a prime candidate for the absorber layers in photovoltaic devices for use in extraterrestrial environments due to its good photovoltaic efficiency and its ability to withstand radiation damage. Efficiencies of up to 19.9% have

been achieved in the laboratory [1] and CIS-based modules are now being produced commercially with efficiencies of around 11.5% [2].

Investigations into radiation damage in these materials have largely concentrated on electron and proton irradiation of thin films and solar cells – particularly to explore the effects on photovoltaic properties [3–35]. Extraterrestrial testing of CIGS-based devices has also been conducted [29,36–43] and work using ion irradiation either to explore lattice damage and/or doping has been performed on single crystals and thin films [7,17,21,32,44–64]. In particular, work by Mullan et al. using oxygen and neon ions has looked at both electrical and structural effects including transmission electron microscopy (TEM) of ion irradiated samples [17,21,45,46,49,50].

In non-irradiated CIS, structural defects have been reported in thin films (stacking faults and microtwins on {112} planes [65–68], dislocations and dislocation loops [66–70]) and in Bridgman-grown single crystals (dislocations on {110} planes [65]). Ion irradiation has been found to induce microtwins, stacking faults, dislocations, dislocation loops and amorphisation [17,45,46,71].

In order to gain an understanding of the atomistic mechanisms which give rise to the radiation hardness of CIS, TEM with in situ ion irradiation has been used in this study as this technique enables the internal microstructure of a sample to be imaged during irradiation thus allowing the exploration of dynamic effects (i.e. not just end-state) whilst also controlling and maintaining variables such as temperature. By using heavy inert ions, in this case Xe, at an energy such that they cause large numbers of atomic displacements throughout the thickness of the sample it is possible to monitor both the creation of structural damage and any recovery processes.

2   Experimental

2.1   *Sample Preparation and Analysis*

Copper, indium and selenium were sealed in evacuated quartz-ampoules which were then heated in a rocking furnace to form CIS via direct fusion of the elements. Single crystals of CIS were produced by refining this material using the Bridgman technique [72]. TEM samples were made by core-drilling material from the bulk, back-polishing, dimpling and then ion beam milling to electron transparency. Sample composition was examined using a

JEOL JSM-6400 SEM equipped with a Link Analytical LZ-5 energy dispersive spectrometer (EDS).

2.2 Transmission Electron Microscopy

Samples were irradiated at room temperature with 400 keV Xe ions in the Intermediate Voltage Electron Microscope (IVEM) at Argonne National Laboratory, USA. The electron beam was operated at 100 kV and remained on during ion irradiation to allow video recording of the experiments. The IVEM facility consists of an Hitachi H-9000NAR coupled to an ion beamline with two sources capable of operating at up to 300 kV and 2 MeV with the ion beam forming an angle of 30° with the optical axis of the microscope [73–75].

Defect analysis was performed using a JEOL JEM-200CX at the University of Salford, United Kingdom. Scanning TEM (STEM) EDS was performed using a FEI CM200 at the University of Leeds, United Kingdom.

Experimental zone-axis pattern maps (ZAPMaps) were produced by tilting along major Kikuchi lines and recording the electron diffraction patterns of major zone-axes. Theoretical zone-axis patterns produced using JAVA Electron Microscopy Software (JEMS) [76,77] were used to identify and verify the experimental patterns. JEMS was also used in the indexing of diffraction spots and Kikuchi lines. All angles were calculated assuming $a = 5.789$ Å and $c = 11.612$ Å [65].

The habit plane of the dislocation loops was identified using $\boldsymbol{g}.\boldsymbol{b}$ analysis techniques. Electron micrographs were taken using underfocused bright-field two-beam imaging conditions for both $\boldsymbol{g}$ and $-\boldsymbol{g}$ for each diffraction vector of interest and with a positive deviation parameter ($s_{\boldsymbol{g}} > 0$). For a sample orientation where $\boldsymbol{g}.\boldsymbol{b} = 0$ (i.e. the Burgers vector of the dislocation loop is at a right angle to the diffraction vector) the diffraction contrast caused by the strain field of the loop will be zero as the distortion of the surrounding planes will be orthogonal to the direction required to bend the planes into the Bragg condition. Conversely for $\boldsymbol{g}.\boldsymbol{b} = 1$ conditions, the strain field around the loop contorts the matrix in the correct manner in order to strongly-excite Bragg diffraction. By establishing two non-parallel diffraction vectors for which the $\boldsymbol{g}.\boldsymbol{b} = 0$ condition exists, it is possible to identify the habit plane and thus calculate the Burgers vector of a dislocation loop. See references [78–80] for further details.

In this study the chalcopyrite structure only featured one diffraction vector which was at 90° to the Burgers vector within the confines of sample orientation and available tilt of the

TEM sample rod. Therefore, diffraction vectors at 82.2° and 82.5° to the Burgers vector were used as these come close to the ideal 90° angle required for an absolute $g.b = 0$ condition. Although technically two $g.b = 0$ conditions are sufficient, one $g.b = 0$ and two $g.b \approx 0$ conditions were used in order to ensure correct identification of the habit plane and Burgers vector.

In order to determine whether the loops were interstitial (extrinsic) or vacancy (intrinsic) in nature, the inside/outside contrast technique was utilised. For a given combination of diffraction vector direction and sign of deviation parameter there will be a particular sense of planar rotation required to approach the Bragg condition. Only certain regions of the strain field around a dislocation loop will bend the planes of the surrounding crystal towards the Bragg condition and this causes diffraction contrast to be generated either on the inside or the outside of the projection of the dislocation loop. This is illustrated in Figure 1 where the direction of planar distortion is indicated for four different combinations of loop nature and inclination. Also shown are two combinations of diffraction vector and deviation parameter with the direction of planar rotation required to approach the Bragg condition indicated for each situation. Comparison of the rotation required to approach the Bragg condition with the rotation due to the strain fields around the loops reveals that diffraction contrast will form inside the projection of the dislocation for the examples on the left of the diagram and outside for those on the right.

Once the habit plane of a dislocation loop is known then the direction of inclination can be determined using knowledge of the crystallography, sample orientation and the mechanical tilt performed using the goniometer and TEM sample rod. Then by reversing the diffraction vector or deviation parameter it is possible to establish the nature of a loop by comparing the images produced and noting the relative shift in the position of the diffraction contrast. See references [78–80] for further details.

3   Results

3.1   *Zone-Axis Pattern Maps*

The experimental ZAPMaps produced to facilitate the characterisation of dislocation loops are shown in Figures 2 and 3. Theoretical patterns were generated by JEMS and used for the identification and verification of the experimental zone-axis patterns. When tilting between zones in the TEM it is useful to know the angles between zones and these can be calculated

using Equation 1 for tetragonal systems such as CIS. The experimental ZAPMaps reproduced here are complimentary to the CIS ZAPMap published previously by Kiely et al. [65] which was cornered on the [001], [021] and [221] zones.

$$\theta = \cos^{-1}\left(\frac{u_1 u_2 + v_1 v_2 + w_1 w_2 \left(\frac{c}{a}\right)^2}{\sqrt{u_1^2 + v_1^2 + \left(\frac{c w_1}{a}\right)^2}\sqrt{u_2^2 + v_2^2 + \left(\frac{c w_2}{a}\right)^2}}\right) \tag{1}$$

3.2   [100] Diffraction Pattern

Table 1 lists the allowed reflections in the chalcopyrite structure of CIS. Comparison with the indexed [100] zone-axis pattern reveals the presence of forbidden reflections as shown in Figure 4. These can be explained by various double-diffraction events such as those listed in Equations 2 to 7. Reflections arising from double diffraction events have also been identified in the [001] and [021] zone-axis patterns of CIS by Kiely et al [65].

$$0\bar{1}1 + 011 = 002 \tag{2}$$
$$0\bar{1}\bar{1} + 01\bar{1} = 00\bar{2} \tag{3}$$
$$0\bar{1}\bar{1} + 013 = 002 \tag{4}$$
$$0\bar{1}1 + 01\bar{3} = 00\bar{2} \tag{5}$$
$$024 + 0\bar{2}\bar{2} = 002 \tag{6}$$
$$02\bar{4} + 0\bar{2}2 = 00\bar{2} \tag{7}$$

Using the fractional coordinates of the atoms in the lattice basis of CIS listed in Table 2, it is possible to calculate the structure factor via Equation 8. The intensity of the 024-type reflections in the [100] zone-axis pattern are comparatively high especially considering their greater angular displacement from the 000 relative to the other reflections shown in Figure 4. This is due to the intensity contributed by the scattering factor of selenium which is reinforcing in these reflections but subtractive in other reflections such as the 020 and 004 as demonstrated in Equations 9 to 11.

$$F(\theta) = \sum_n f_n(\theta) e^{i 2\pi (u_n h + v_n k + w_n l)} \tag{8}$$
$$020: F(\theta) = 3 f_{Cu}(\theta) + 4 f_{In}(\theta) - 8 f_{Se}(\theta) \tag{9}$$
$$004: F(\theta) = 3 f_{Cu}(\theta) + 4 f_{In}(\theta) - 8 f_{Se}(\theta) \tag{10}$$

$$024: F(\theta) = 3f_{\text{Cu}}(\theta) + 4f_{\text{In}}(\theta) + 6f_{\text{Se}}(\theta) \tag{11}$$

3.3   Dislocation Loops

3.3.1   Loop Development

Dislocation loops were found to form in copper-rich indium-poor selenium-rich TEM samples when irradiated at room temperature with 400 keV Xe ions as shown in Figure 5.

Three samples were irradiated to fluences of 1.3×10^{13}, 7.5×10^{13} and 1.3×10^{14} ions.cm^{-2} (corresponding to approximately 0.25, 1.5 and 2.6 displacements per atom at a depth of 50 nm from the irradiated surface, respectively) resulting in typical dislocation loops sizes of 5, 40 and 50 nm, respectively. The loops were seen to form and grow under irradiation and on occasions disappear in a period of less than 1/30$^{\text{th}}$ of a second (one frame of video). On occasions, loops also appeared to merge although it is hard to be definitive based on the evidence of the two-dimensional projection of the regions of the strain fields satisfying the Bragg condition – it can be difficult to conclusively distinguish between two strain fields overlapping in projection and two loops amalgamating. However, as the loops were growing it is highly likely that some would have come sufficiently close to amalgamate. The loops were stable once irradiation ceased. Figure 6 shows dislocation loop evolution in one area over several minutes as a function of fluence.

3.3.2   Habit Plane and Burgers Vector

The sample irradiated to the highest fluence of 1.3×10^{14} ions.cm^{-2}, and hence with the largest defects, was used for determination of dislocation habit plane and Burgers vector. Figure 7 shows eight TEM micrographs which demonstrate the habit plane of the dislocation loops to be {112}. The micrographs taken with $\boldsymbol{g} = 1\bar{1}\bar{2}$ and $\bar{1}12$ produce twin lobed contrast features consistent with end-on loops which are pure edge in character. All six of the diffraction vectors which are orthogonal (or nearly orthogonal) to the $1\bar{1}\bar{2}$ and $\bar{1}12$ result in invisibility of {112}-type loops. This conclusion is further illustrated in Figure 8 using annular dark field (ADF) TEM and in Figure 9 using weak-beam dark-field (WBDF) TEM; both techniques generate contrast corresponding to the most heavily distorted planes which are located closest to the centre of a dislocation loop and thus give better information on the

actual dislocation rather than about the more widely dispersed regions of the associated strain field. As can be seen in Figures 8 and 9, for both ADF and WBDF the observed contrast is consistent with loops residing on the {112} planes.

Based on this habit plane, the Burgers vector can therefore be calculated as $\boldsymbol{b} = 1/6$ <221> as illustrated in Figure 10 using the Finish-Start/Right-Hand (FS/RH) convention.

3.3.2   Loop Nature

The loops were demonstrated to be interstitial in nature. As can be seen in Figure 11, a reversal of the diffraction vector from $1\bar{3}\bar{6}$ to $\bar{1}36$ resulted in a shift from outside to inside contrast which is verified by the intensity-linescan data plotted in Figure 12 for one of the dislocation loops shown in Figure 11. The situation is represented schematically in Figure 13.

3.3.3   Loop Contents

No variation in composition between the contents of the dislocation loops and the surrounding matrix was detected by STEM EDS as demonstrated in Figure 14. The instrument used is estimated to be capable of detecting a variation of 5 at.% in a single end-on interstitial loop of this size. This suggests that the interstitial planes in the loops are close to being stoichiometric – as ideal {112} planes are stoichiometric (containing Cu, In and Se in a ratio of 1:1:2) this is not an unreasonable situation. No other elements were detected in either the loops or the surrounding matrix.

Additional analysis using electron energy loss spectroscopy on SuperSTEM 2 at Daresbury Laboratory, United Kingdom, also did not detect any variation in composition.

4   Discussion

As the loops grew and did not appear instantaneously, they must have formed through the agglomeration of point defects or defect clusters rather than forming as the remnants of individual collision cascades. The most likely causes for the sudden disappearance of any given dislocation loop was the proximity of a surface (a situation reached through loop growth or migration) or the disordering effects of a nearby ion induced collision cascade and thermal spike.

Because the loops were extrinsic in nature they must have been formed through the agglomeration of mobile interstitial defects. However, this raises the question as to the fate of the vacancies whose creation must necessarily have been concurrent with that of the interstitials which went on to constitute the loops. Vacancies could be are relatively immobile in CIS and/or they could have become entangled in defect complexes as discussed below. The migration mechanisms for copper, indium and selenium in CIS are not completely understood with the literature containing a complex picture featuring a range of proposed mechanisms and migration energies often influenced by composition [81–115]. However, despite the ambiguities in this area it is clear that selenium is immobile at room temperature by any migration mechanism and therefore so too must its vacancies [81,105–107].

Zhang et al have calculated creation energies for a range of defect complexes from first principles and found the formation of $2V_{Cu}^{-}+In_{Cu}^{2+}$ to have a particularly low energy [116–121]. Other work by Klais et al has predicted $2V_{Cu}+In_{Cu}$ to be abundant throughout the compositions they considered and also found experimental evidence for its existence through positron annihilation [122]. Therefore it is quite possible that the copper vacancies could be become entangled in complexes such as the $2V_{Cu}+In_{Cu}$ which requires three V_{Cu}. Unfortunately, the $2V_{Cu}+In_{Cu}$ does not explain the fate of the indium vacancies. These could have similarly been immobilised by V_{In} consuming complexes with relative low creation energies such as: $Cu_{In}+2Cu_i$ [123,124]; $Cu_{In}+V_{Se}$ [120]; $Se_{Cu}+Se_{In}$ [125]; or any of $Cu_{In}+Cu_i+V_{Se}$, $Cu_{In}+V_{Cu}$, $Cu_{In}+V_{Cu}+V_{Se}$ and $V_{Se}+Cu_{In}$ [122].

As the samples in which dislocation loops were observed were slightly selenium rich it is also quite possible that the selenium vacancy population was suppressed by this excess – a similar argument works for copper but not for indium due to the composition of the samples studied. However, the indium vacancy population could have been suppressed by a copper excess as the Cu_{In} antisite defect has been calculated to have a relatively low creation energy of between 1.11 and 1.54 eV [120,126–129] (although there is one out-lying value of 1.90 eV [130]).

5   Conclusions

Dislocation loops were formed in CIS using 400 keV Xe ions at room temperature. These loops were interstitial in nature as shown through inside/outside contrast inversion and resided on {112} planes as demonstrated using ***g.b***, weak beam dark field and annular dark

field techniques. The Burgers vector has been calculated as $b = 1/6 <221>$. The loops grew through the agglomeration of mobile interstitial defects. They sometimes disappeared instantaneously either due to a local ion induced collision cascade and thermal spike or by growing/migrating into the proximity of a surface. Whilst the interstitials produced by displacing radiation clearly formed dislocation loops, the fate of the vacancies requires further study but could have been suppressed by the excess copper and selenium in the sample composition and/or entanglement in the defect complexes known to offer stable structures in defected CIS.

Acknowledgements

References

[1]   I. Repins, M. Contreras, M. Romero, Y. Yan, W. Metzger, J. Li, S. Johnston, B. Egass, C. DeHart, J. Scharf, B.E. McCandless and R. Noufi, *Characterization of 19.9% Efficient CIGS Absorbers*, 33rd IEEE Photovolt. Specialists Conf., San Diego, California, USA (2008).

[2]   M. Powalla and D. Bonnet, Adv. in Optoelectron. 2007 (2007).

[3]   H.-S. Lee, H. Okada, A. Wakahara and A. Yoshida, J. Appl. Phys. 94 (2003) p.276.

[4]   R.M. Burgess, W.S. Chen, W.E. Devaney, D.H. Doyle, N.P. Kim and B.J. Stanbery, 20th IEEE Photovolt. Specialists Conf., (1988) p.909.

[5]   H. Okada, H.S. Lee, A. Wakahara, A. Yoshida, T. Ohshima and T. Kamiya, Sol. Energ. Mat. Sol. Cell 90 (2006) p.93.

[6]   A. Polity, R. Krause-Rehberg, T.E.M. Staab, M.J. Puska, J. Klais, H.J. Möller and B.K. Meyer, J. Appl. Phys. 83 (1998) p.71.

[7]   L.L. Kazmerski, N.A. Burnham, A.B. Swartzlander, A.J. Nelson and S.E. Asher, 19th IEEE Photovolt. Specialists Conf., (1987) p.1315.

[8]   A. Jasenek and U. Rau, J. Appl. Phys. 90 (2001) p.650.

[9]   A. Jasenek, A. Boden, K. Weinert, M.R. Balboul, H.W. Schock and U. Rau, Mat. Res. Soc. Symp. Proc. 668 (2001) p.H3.2.1.

[10]   A. Jasenek, U. Rau, T. Hahn, G. Hanna, M. Schmidt, M. Hartmann, H.W. Schock, J.H. Werner, B. Schattat, S. Kraft, K.-H. Schmid and W. Bolse, Appl. Phys. A: Solids Surf. 70 (2000) p.677.

[11]   A. Jasenek, U. Rau, K. Weinert, H.W. Schock and J.H. Werner, Appl. Phys. Lett. 82 (2003) p.1410.

[12]   B.J. Stanbery, J.E. Avery, R.M. Burgess, W.S. Chen, W.E. Devaney, D.H. Doyle, R.A. Mickelsen, R.W. McClelland, B.D. King, R.P. Gale and J.C.C. Fan, 19th IEEE Photovolt. Specialists Conf., (1987) p.280.

[13]   C.F. Gay, R.R. Potter and D. Tanner, 17th IEEE Photovolt. Specialists Conf., (1984) p.151.

[14]   T. Hisamatsu, T. Aburaya and S. Matsuda, 2nd World Conf. Exhib. Photovolt. Sol. Energ. Convers. (1998) p.3568.

[15]   H.-S. Lee, H. Okada, A. Wakahara, T. Ohshima, H. Itoh, S. Kawakita, M. Imaizumi, S. Matsuda and A. Yoshida, J. Phys. Chem. Solids 64 (2003) p.1887.

[16]   T. Tanaka, T.H. Yamaguchi, A. Wakahara, A. Yoshida, R. Taniguchi, Y. Matsuda and M. Fujishiro, Sol. Energ. Mat. Sol. Cell 75 (2003) p.115.

[17]   C.A. Mullan, C.J. Kiely, M. Yakushev, M. Imanieh, R.D. Tomlinson and A. Rockett, Microsc. Semicond. Mat. Conf. 134 (1993) p.547.

[18]   K. Otte, G. Lippold, H. Neumann and A. Schindler, J. Phys. Chem. Solids 64 (2003) p.1641.

[19]   M.V. Yakushev, P.A. Jones, H. Neumann, G.A. Stephens and R.D. Tomlinson, Nucl. Instrum. Methods Phys. Res. B 84 (1994) p.405.

[20]   M.V. Yakushev, G. Lippold, A.E. Hill, R.D. Pilkington and R.D. Tomlinson, Cryst. Res. Technol. S31 (1996) p.357.

[21]   R.D. Tomlinson, A.E. Hill, G.A. Stephens, M. Imanieh, P.A. Jones, R.D. Pilkington, P. Rimmer, M.V. Yakushev and H. Neumann, 11th Euro. Photovolt. Sol. Energ. Conf., Montreux, Switzerland (1992) p.791.

[22]   H.-S. Lee, H. Okada, A. Wakahara, A. Yoshida, T. Ohshima, H. Itoh, S. Kawakita, M. Imaizumi and S. Matsuda, Sol. Energ. Mat. Sol. Cell 75 (2003) p.57.

[23]   Y. Akaki, N. Ohryoji, A. Fukuyama, K. Yoshino, S. Kawakita, M. Imaizumi, S. Niki, K. Sakurai, S. Ishizuka, T. Ohshima and T. Ikari, Thin Solid Films 480–481 (2005) p.250.

[24]   Y. Akaki, N. Ohryoji, K. Yoshino, S. Kawakita, M. Imaizumi, N. Shigeru, K. Sakurai, S. Ishizuka, T. Ohshima and T. Ikari, Solid-State Electron. 48 (2004) p.1815.

[25]   Y. Akaki, K. Yoshino, T. Ikari, S. Kawakita and M. Imaizumi, Appl. Phys. Lett. 85 (2004) p.1347.

[26]   S. Kawakita, M. Imaizumi, M. Yamaguchi, K. Kushiya, T. Ohshima, H. Itoh and S. Matsuda, Jpn. J. Appl. Phys. 41 (2002) p.L797.

[27]   H. Dursch, W. Chen and D. Russell, Space Photovolt. Res. Technol. Conf. (1985) p.165.

[28] R.A. Mickelsen, W.S. Chen, B.J. Stanbery, H. Dursch, J.M. Stewart, Y.R. Hsiao and W. Devaney, 18th IEEE Photovolt. Specialists Conf. (1985) p.1069.

[29] H.W. Schock and K. Bogus, 2nd World Conf. Exhib. Photovolt. Sol. Energ. Convers., Vienna, Austria (1998) p.3586.

[30] H. Scheel, G. Frank and H.P. Strunk, Phys. Status Solidi A 202 (2005) p.2336.

[31] K. Weinert, A. Jasenek and U. Rau, Thin Solid Films 431–432 (2003) p.453.

[32] Y. Yan, K.M. Jones, R. Noufi and M.M. Al-Jassim, Thin Solid Films 515 (2007) p.4681.

[33] A. Jasenek, U. Rau, K. Weinert, I.M. Kötschau, G. Hanna, G. Voorwinden, M. Powalla, H.W. Schock and J.H. Werner, Thin Solid Films 387 (2001) p.228.

[34] A. Rao, S. Krishnan, G. Sanjeev, K. Siddappa, H.S. Ullal and X. Wu, Sol. Energ. Mat. Sol. Cell 93 (2009) p.1618.

[35] U. Rau, A. Jasenek, H.W. Schock, J.H. Werner, G. La Roche, A. Robben and K. Bogus, 28th IEEE Photovolt. Specialists Conf. (2000) p.1032.

[36] R.M. Burgess, W.E. Devaney and W.S. Chen, 24th IEEE Photovolt. Specialists Conf. (1993) p.1465.

[37] H. Curtis and D. Marvin, 25th IEEE Photovolt. Specialists Conf. (1996) p.195.

[38] D.A. Guidice, K.P. Ray, H.B. Curtis and D.C. Ferguson, 31st Intersoc. Energ. Convers. Eng. Conf. (1996) p.7.

[39] D.A. Guidice, P.S. Severance and K.C. Reinhardt, 11th Space Photovolt. Res. Technol. Conf. (1991) p.33.

[40] M. Imaizumi, T. Sumita, S. Kawakita, O. Anzawa and S. Matsuda, 18th Space Photovolt. Res. Technol. Conf. (2005) p.24.

[41] M. Imaizumi, T. Sumita, S. Kawakita, K. Aoyama, O. Anzawa, T. Aburaya, T. Hisamatsu and S. Matsuda, Prog. Photovolt.: Res. Appl. 13 (2005) p.93.

[42] G. La Roche, B. Hoesselbarth and K. Bogus, 16th Euro. Photovolt. Sol. Energ. Conf. (2000) p.945.

[43] J.G. Severns, R.M. Hobbs, N.P. Elliott, R.H. Towsley, R.W. Conway and G.F. Virshup, 20th IEEE Photovolt. Specialists Conf. (1988) p.801.

[44] G. Lippold, K. Otte, H. Schlemm and W. Grill, Mat. Res. Soc. Symp. Proc. 513 (1998) p.269.

[45] C.A. Mullan, C.J. Kiely, A. Rockett, M. Imanieh, M.V. Yakushev and R.D. Tomlinson, Mat. Res. Soc. Symp. Proc. 262 (1992) p.1097.

[46] C.A. Mullan, C.J. Kiely, M.V. Yakushev, M. Imanieh, R.D. Tomlinson and A. Rockett, Phil. Mag. A 73 (1996) p.1131.

[47] K. Otte, G. Lippold, D. Hirsch, A. Schindler and F. Bigl, Thin Solid Films 361–362 (2000) p.498.

[48] D. Fink, J. Krauser, G. Lippold, M.V. Yakushev, R.D. Tomlinson, A. Weidinger, K.K. Dwivedi, S. Ghosh and W.H. Chung, Radiat. Eff. Defects Solids 145 (1998) p.85.

[49]   R.D. Tomlinson, A.E. Hill, M. Imanieh, R.D. Pilkington, A. Roodbarmohammadi, M.A. Slifkin and M.V. Yakushev, J. Electron. Mat. 20 (1991) p.659.

[50]   V.P. Crowther, M. Imanieh, G.A. Stephens and R.D. Tomlinson, Nucl. Instrum. Methods Phys. Res. B 67 (1992) p.428.

[51]   K. Otte, G. Lippold, F. Frost, A. Schindler, F. Bigl, M.V. Yakushev and R.D. Tomlinson, J. Vac. Sci. Technol. A 17 (1999) p.19.

[52]   M. Nishitani, T. Negami, S. Kohiki, M. Terauchi, H. Wada and T. Hirao, J. Appl. Phys. 74 (1993) p.2067.

[53]   T. Tanaka, A. Wakahara, A. Yoshida, T. Ohshima, H. Itoh and S. Okada, J. Appl. Phys. 87 (2000) p.3283.

[54]   S. Kohiki, N. Mikihiko, T. Negami and H. Wada, Appl. Phys. Lett. 62 (1993) p.1656.

[55]   S. Kohiki, M. Nishitani, T. Negami and T. Wada, Thin Solid Films 226 (1993) p.149.

[56]   T. Tanaka, T. Yamaguchi, T. Ohshima, H. Itoh, A. Wakahara and A. Yoshida, Sol. Energ. Mat. Sol. Cell 75 (2003) p.109.

[57]   P.W. Yu, Y.S. Park and J.T. Grant, Appl. Phys. Lett. 28 (1976) p.214.

[58]   T.P. Massopust, P.J. Ireland, L.L. Kazmerski and K.J. Bachmann, J. Vac. Sci. Technol. A 2 (1984) p.1123.

[59]   P. Corvini, A. Kahn and G. Wagner, J. Appl. Phys. 57 (1985) p.2967.

[60]   A. Kahn, P. Corvini, S. Wagner and K.J. Bachmann, Solar Cells 16 (1986) p.123.

[61]   K. Weinert, M. Lippold, M.V. Yakushev, R.D. Tomlinson, R. Klenk and V. Nadenau, 2nd World Conf. Exhib. Photovolt. Sol. Energ. Convers. (1998) p.3679.

[62]   P.W. Yu, J.T. Grant, Y.S. Park and T.W. Haas, J. Appl. Phys. 48 (1977) p.67.

[63]   P.W. Yu, Y.S. Park, S.P. Faile and J.E. Ehret, Appl. Phys. Lett. 26 (1975) p.717.

[64]   G. Lippold, M.V. Yakushev, R.D. Tomlinson, A.E. Hill and W. Grill, Cryst. Res. Technol. S31 (1996) p.381.

[65]   C.J. Kiely, R.C. Pond, G. Kenshole and A. Rockett, Phil. Mag. A 63 (1991) p.1249.

[66]   J.H. Schön, J. Albert and E. Bucher, Thin Solid Films 301 (1997) p.115.

[67]   B.-H. Tseng, A. Rockett, T. Lommasson, L.C. Yang, C.A. Wert and J.A. Thornton, J. Appl. Phys. 67 (1990) p.2637.

[68]   A.N. Tiwari, M. Krejci, F.-J. Haug and H. Zogg, Thin Solid Films 361–362 (2000) p.41.

[69]   H.Z. Xiao, L.-C. Yang and A. Rockett, J. Appl. Phys. 76 (1994) p.1503.

[70]   M.H. Bode, M.M. Al-Jassim, J. Tuttle and D. Albin, Mat. Res. Soc. Symp. Proc. 283 (1993) p.927.

[71]   S.E. Donnelly, J.A. Hinks, P.D. Edmondson, R.D. Pilkington, M. Yakushev and R.C. Birtcher, Nucl. Instrum. Methods Phys. Res. B 242 (2006) p.686.

[72]   P.W. Bridgman, Proc. Am. Acad. Arts Sci. 60 (1925) p.315.

[73]   C.W. Allen, Ultramicroscopy 56 (1994) p.200.

[74]   C.W. Allen, L.L. Funk and E.A. Ryan, Mater. Res. Soc. Symp. Proc. 396 (1996) p.641.

[75]   R.C. Birtcher, M.A. Kirk, K. Furuya, G.R. Lumpkin and M.O. Ruault, J. Mater. Res. 20 (2005) p.1654.

[76]   P.A. Stadelmann, Ultramicroscopy 21 (1987) p.131.

[77]   P. Stadelmann, *Electron Microscopy Software Java Version (JEMS)* v2.0105W2005 (2005).

[78]   J.W. Edington, *Practical Electron Microscopy In Materials Science*, N.V. Philips Gloeilampenfabrieken, Eindhoven, 1976.

[79]   M.L. Jenkins and M.A. Kirk, *Characterization of Radiation Damage by Transmission Electron Microscopy*, Institute of Physics Publishing, London, 2001.

[80]   D.B. Williams and C.B. Carter, *Transmission Electron Microscopy: a Textbook for Materials Science*, Plenum Press, New York, 1996.

[81]   J. Parkes, R.D. Tomlinson and M.J. Hampshire, J. Cryst. Growth 20 (1973) p.315.

[82]   D. Cahen, J.-M. Gilet, C. Schmitz, L. Chernyak, K. Gartsman and A. Jakubowicz, Science 258 (1992) p.271.

[83]   I. Shih, C.H. Champness and A. Vahid Shahidi, Solar Cells 16 (1986) p.27.

[84]   I. Lubomirsky, M.K. Rabinal and D. Cahen, J. Appl. Phys. 81 (1997) p.6684.

[85]   L. Chernyak, K. Gartsman, D. Cahen and O.M. Stafsudd, J. Phys. Chem. Solids 56 (1995) p.1165.

[86]   D. Soltz, G. Dagan and D. Cahen, Solid State Ionics 28–30 (1988) p.1105.

[87]   M. Kleinfeld and H.D. Wiemhöfer, Solid State Ionics 28–30 (1988) p.1111.

[88]   G. Dagan, F. Abou-Elfotouh, D.J. Dunlavy, R.J. Matson and D. Cahen, Chem. Mater. 2 (1990) p.286.

[89]   G. Dagan, T.F. Ciszek and D. Cahen, J. Phys. Chem. 96 (1992) p.11009.

[90]   D. Cahen, L. Chernyak, G. Dagan and A. Jakubowicz, *Ion mobility in chalcogenide semiconductors; room temperature creation of bipolar junction transistor* in *Fast Ion Transport in Solids* (1993) p.121.

[91]   B. Tell and P.M. Bridenbaugh, J. Appl. Phys. 48 (1977) p.2477.

[92]   K. Gartsman, L. Chernyak, V. Lyahovitskaya, D. Cahen, V. Didik, V. Kozlovsky, R. Malkovich, E. Skoryatina and V. Usacheva, J. Appl. Phys. 82 (1997) p.4282.

[93]   G.E. Kenshole, C.J. Li, C.R. Toro and J.J. Loferski, 5th Euro. Photovolt. Sol. Energ. Conf., (1983) p.65.

[94]   P.E. Stallworth, J.-F. Guillemoles, J. Flowers, J. Vedel and S.G. Greenbaum, Solid State Commun. 113 (2000) p.527.

[95]   A.P. Kumar and K.V. Reddy, Semicond. Sci. Technol. 12 (1997) p.966.

[96]   I. Lubomirsky, K. Gartsman and D. Cahen, J. Appl. Phys. 83 (1998) p.4678.

[97]   S.M.F. Hasan, L. Quadir, K.S. Begum, M.A. Subhan and K.M. Mannan, Vacuum 55 (1999) p.17.

[98]   J.C.W. Bates, K.F. Nelson, S. Atiq Raza, J.B. Mooney, J.M. Recktenwald, L. Macintosh and R. Lamoreaux, Thin Solid Films 88 (1982) p.279.

[99]   A. Virtuani, E. Lotter, M. Powalla, U. Rau, J.H. Werner and M. Acciarri, J. Appl. Phys. 99 (2006) p.014906.

[100]   T. Yamaguchi, J. Matsufusa and A. Yoshida, Sol. Energ. Mat. Sol. Cell 27 (1992) p.25.

[101]   E. Niemi and L. Stolt, Surf. Interface Anal. 15 (1990) p.422.

[102]   M. Marudachalam, R.W. Birkmire, H. Hichri, J.M. Schultz, A. Swartzlander and M.M. Al-Jassim, J. Appl. Phys. 82 (1997) p.2896.

[103]   M. Marudachalam, H. Hichri, R.W. Birkmire and J.M. Schultz, 25th IEEE Photovolt. Specialists Conf. (1996) p.805.

[104]   K. Djessas, S. Yapi, G. Massé, M. Ibannain and J.L. Gauffier, J. Appl. Phys. 95 (2004) p.4111.

[105]   A.P. Kumar and K.V. Reddy, Thin Solid Films 304 (1997) p.365.

[106]   C.H. Champness and G.I. Ahmad, Thin Solid Films 361–362 (2000) p.482.

[107]   C.H. Champness and G.I. Ahmed, J. Vac. Sci. Technol. A 18 (2000) p.693.

[108]   H.J. von Bardeleben, J. Appl. Phys. 56 (1984) p.321.

[109]   K.D. Becker and S. Wagner, Phys. Rev. B 27 (1983) p.5240.

[110]   G.A. Medvedkin, M.M. Sobolev and S.A. Solovjev, J. Appl. Phys. 82 (1997) p.5167.

[111]   V. Nádaždy, M.V. Yakushev, E.H. Djebbar, A.E. Hill and R.D. Tomlinson, J. Appl. Phys. 84 (1996) p.4322.

[112]   A. Rockett, *Fundamental Studies of the Effect of Crystal Defects on CuInSe2/CdS Heterojunction Behavior – Final Report 28 June 1993 – 30 June 1998*, National Renewable Energy Laboratory (1999).

[113]   D.J. Schroeder, G.D. Berry and A.A. Rockett, Appl. Phys. Lett. 69 (1996) p.4068.

[114]   O. Lundberg, J. Lu, A. Rockett, M. Edoff and L. Stolt, J. Phys. Chem. Solids 64 (2003) p.1499.

[115]   S. Wagner, Proc. Electrochem. Soc. 83 (1983) p.410.

[116]   S.-H. Wei and S.B. Zhang, J. Phys. Chem. Solids 66 (2005) p.1994.

[117]   S.-H. Wei, S.B. Zhang and A. Zunger, 11th Int. Conf. Ternary Multinary Compd. (1997) p.765.

[118]   S.-H. Wei, S.B. Zhang and A. Zunger, Appl. Phys. Lett. 72 (1998) p.3199.

[119]   S.B. Zhang, S.-H. Wei and A. Zunger, Phys. Rev. Lett. 78 (1997) p.4059.

[120]   S.B. Zhang, S.-H. Wei, A. Zunger and H. Katayama-Yoshida, Phys. Rev. B 57 (1998) p.9642.

[121]   A. Zunger, S.B. Zhang and S.-H. Wei, 26th IEEE Photovolt. Specialists Conf. (1997) p313.

[122]   J. Klais, H.J. Möller and D. Cahen, Thin Solid Films 361–362 (2000) p.446.

[123]   H.H. Chang, H.Y. Ueng and H.L. Hwang, Mater. Sci. Semicond. Process. 6 (2003) p.401.

[124]   H.-H. Chang, H.Y. Ueng and H.L. Hwang, J. Phys. Chem. Solids 64 (2003) p.2047.

[125] F. Abou-Elfotouh, D.J. Dunlavy and T.J. Coutts, Solar Cells 27 (1989) p.237.

[126] C. Domain, S. Laribi, S. Taunier and J.F. Guillemoles, J. Phys. Chem. Solids 64 (2003) p.1657.

[127] J.-F. Guillemoles, Thin Solid Films 361–362 (2000) p.338.

[128] H. Neumann, *I-III-VI$_2$-Halbleiter$_2$* in *Verbindungshalbeiter* (1986) p.392.

[129] C. Rincón, C. Bellabarba, J. González and G. Sánchez Pérez, Solar Cells 16 (1986) p.335.

[130] H.J. Möller, Solar Cells 31 (1991) p.77.

Table 1: Allowed reflections, derivable from Table 2 and Equation 8, in the chalcopyrite structure of CIS where h, k and l are the non-zero Miller indices and n is an integer.

Reflection	Condition
hkl	$h + k + l = 2n$
$hk0$	$h + k = 2n$
$0kl$	$k + l = 2n$
hhl	$2h + l = 4n$
$00l$	$l = 4n$
$h00$	$h = 2n$
$h\bar{h}0$	$h = 2n$

Table 2: Fractional coordinates of the atoms in the lattice basis of CIS where u, v and w are fractions of the lattice parameters a, b and c, respectively.

	u	*v*	*w*
Copper	0	0	0
	0	0.5	0.25
	0.5	0.5	0.5
	0.5	0	0.75
Indium	0.5	0.5	0
	0.5	0	0.25
	0	0	0.5
	0	0.5	0.75
Selenium	0.25	0.25	0.125
	0.75	0.75	0.125
	0.75	0.25	0.375
	0.25	0.75	0.375
	0.25	0.25	0.625
	0.75	0.75	0.625
	0.75	0.25	0.875
	0.25	0.75	0.875

Inside contrast   Outside contrast

Electron beam

(a)

(b)

(c)

Position of diffraction contrast (————) in image relative to dislocation (– – –)

g g

s_g (d) s_g

K K
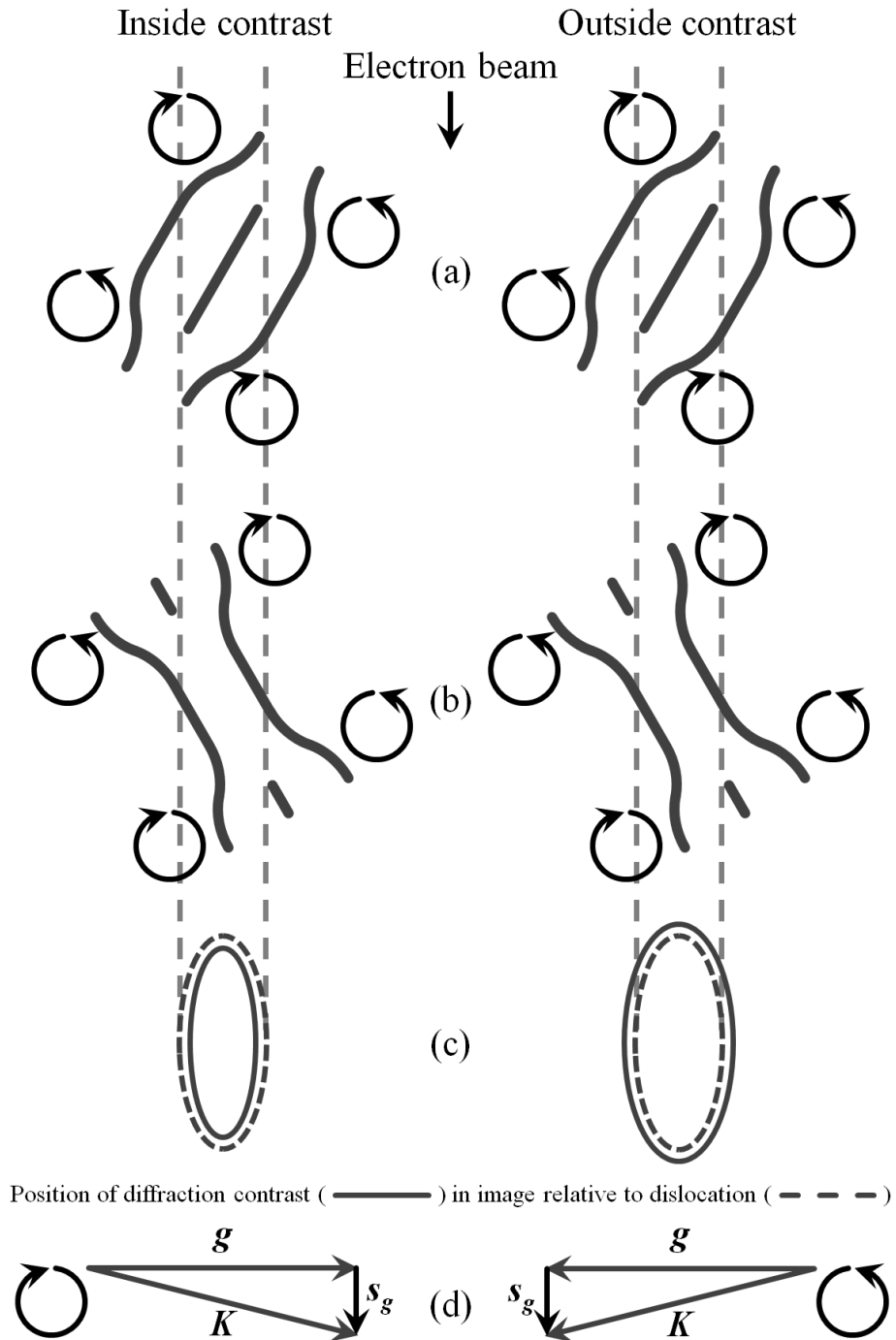
Figure 1: Schematic diagram showing the directions in which the planes of a crystal are rotated by the strain fields of (a) interstitial loops and (b) vacancy loops; (d) illustrates the direction in which the sample must be rotated in order for the deviation parameter (s_g) to be reduced such that these distorted planes approach the Bragg condition (i.e. diffraction vector, g, approaches the scattering wavevector, K). This causes diffraction contrast to be formed on the inside of the dislocation loop for the situations depicted on the left and on the outside for those on the right as shown in (c) (after [78,80]).
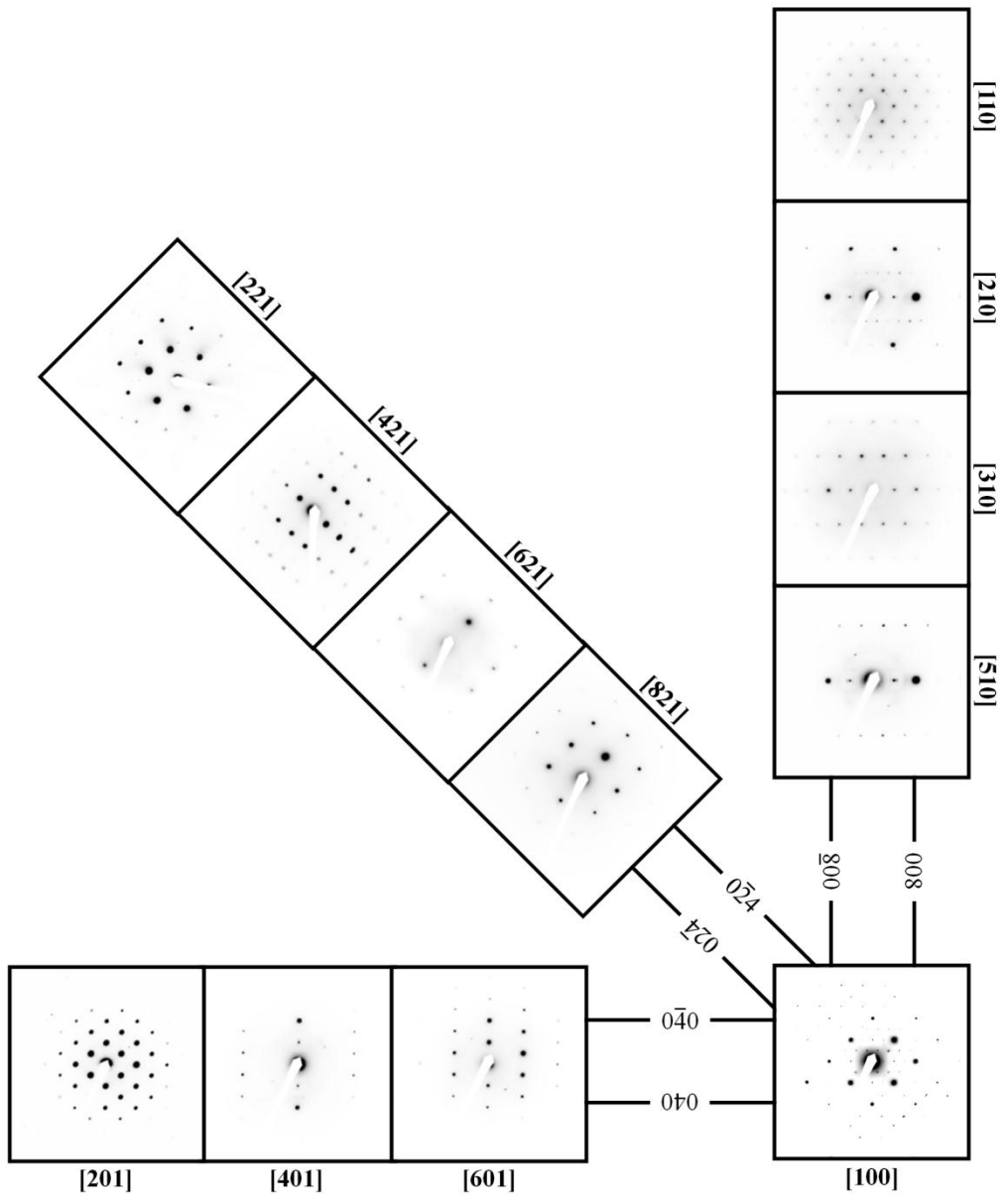
Figure 2: Quadrant of experimental [100]-centred ZAPMap.
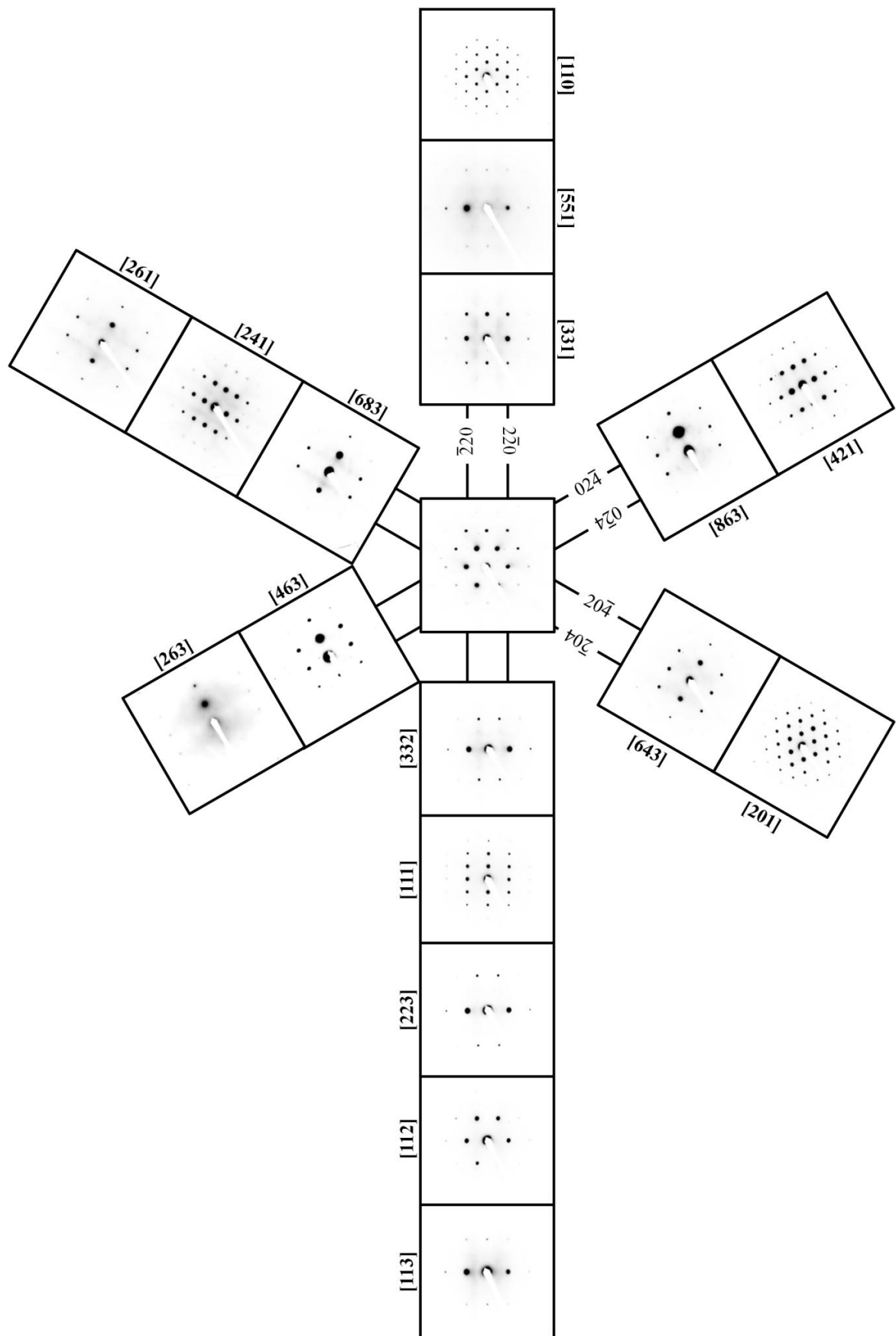
Figure 3: Experimental [221]-centred ZAPMap.
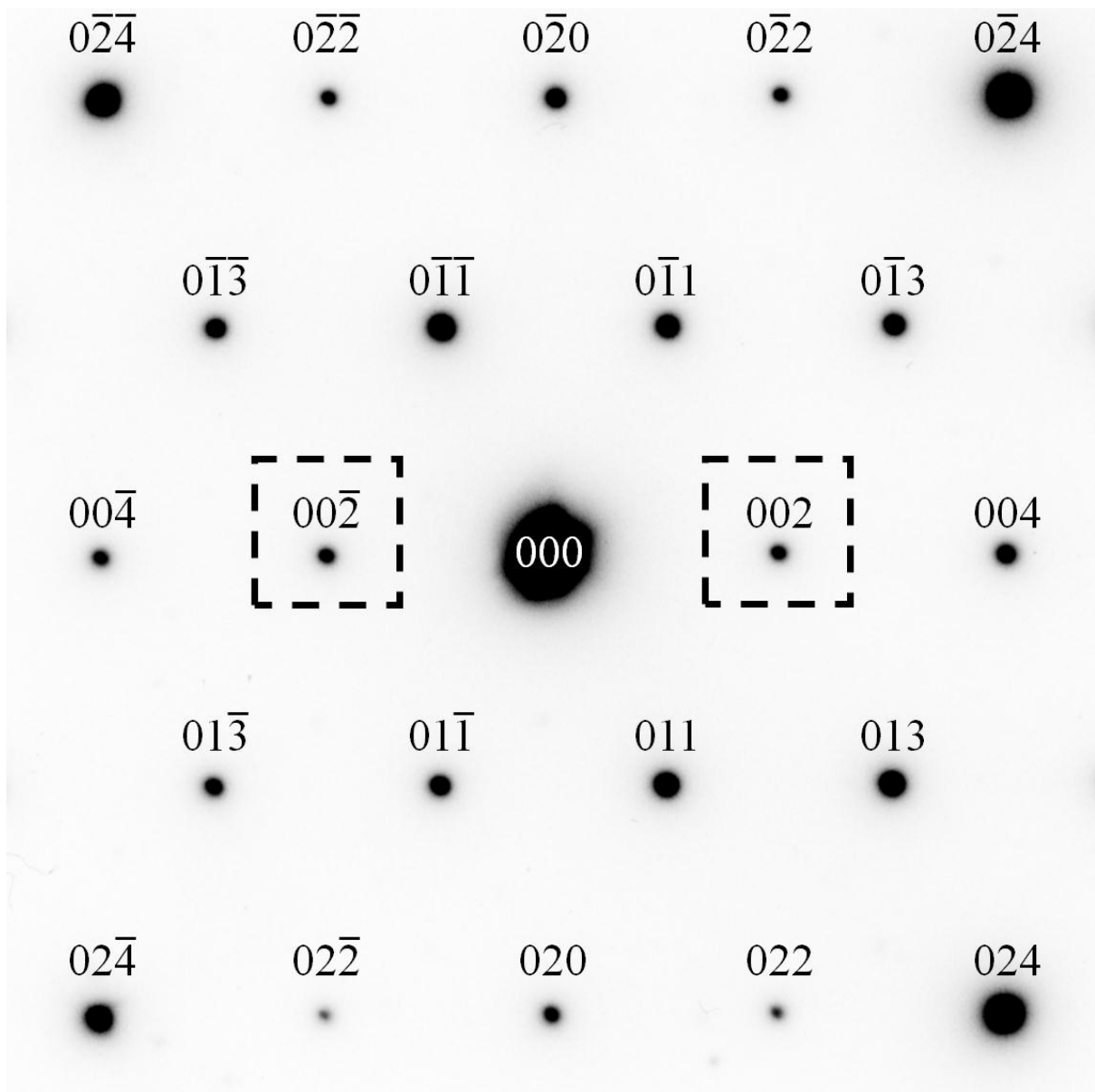
Figure 4: Indexed experimental diffraction pattern of the [100]-zone with reflections forbidden by structure factor considerations indicated with dashed boxes.
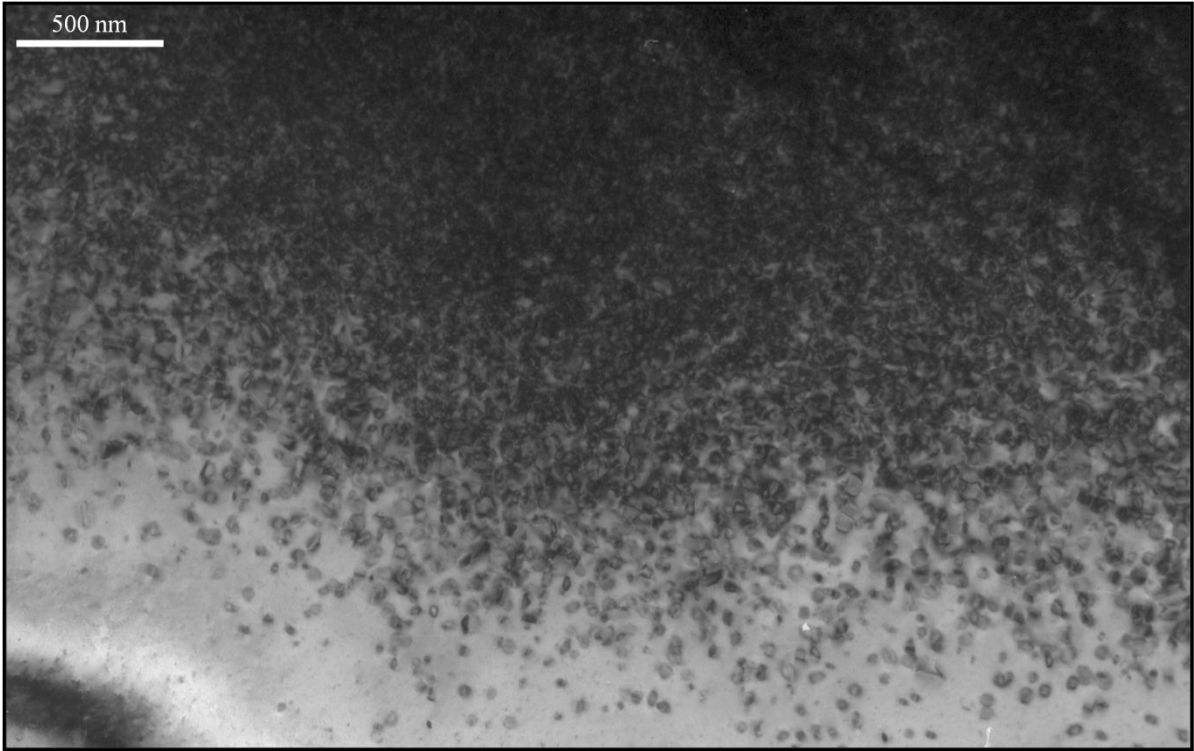
Figure 5: Underfocus bright-field down-zone TEM micrograph of radiation induced dislocation loops in CIS. The areal density of the defects increased with sample thickness with the thinnest areas towards the bottom of the image being too thin to accommodate loops.

(a) 5×10^{13} ions.cm^{-2} at $t = 0$ s

(b) 6×10^{13} ions.cm^{-2} at $t = 70$ s

(c) 7×10^{13} ions.cm^{-2} at $t = 141$ s

(d) 8×10^{13} ions.cm^{-2} at $t = 208$ s

(e) 9×10^{13} ions.cm^{-2} at $t = 273$ s

(f) 10^{14} ions.cm^{-2} at $t = 339$ s

(g) 1.1×10^{14} ions.cm^{-2} at $t = 404$ s

(h) 1.2×10^{14} ions.cm^{-2} at $t = 468$ s
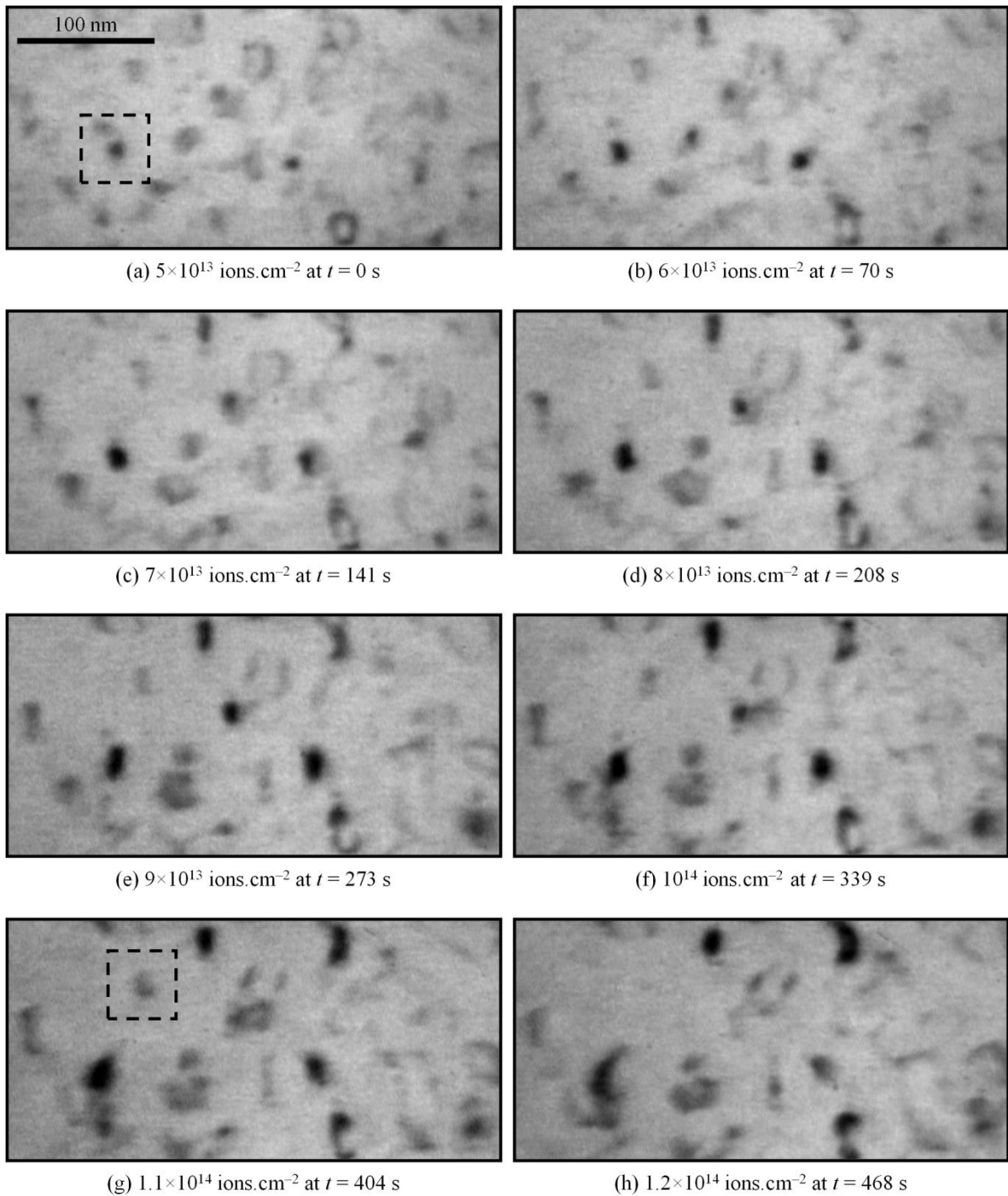
Figure 6: Underfocus bright-field down-zone TEM micrographs showing the development of ion beam induced dislocation loops under continued ion irradiation. Attention is drawn to examples of loop growth (follow defect highlighted with dashed box in panel (a)) and destruction (follow defect highlighted with dashed box in panel (g)). Scale marker applies to all eight micrographs.
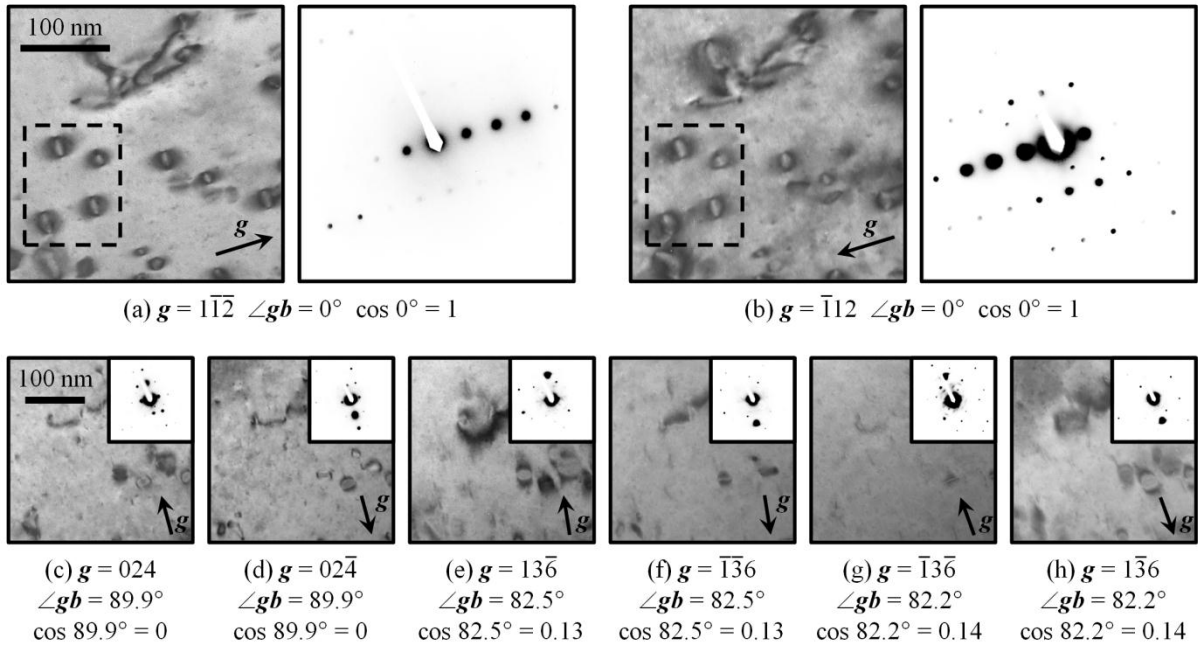
Figure 7: Underfocus bright-field two-beam TEM micrographs ($s_g > 0$) showing determination of dislocation loop habit plane using g.b analysis. Attention is drawn to the four dislocation loops highlighted by the dashed boxes in micrographs (a) and (b) as examples of {112}-type loops which lie on the (1$\bar{1}$2) planes as demonstrated by their contrast under the various g.b conditions shown − however, other instances are also evident in these micrographs. Note that there is no inside/outside contrast reversal for {112}-type dislocation loops between the micrographs in (a) and (b) as the loops are not inclined − this is contrary to the situation depicted in Figure 11 where the dislocation loops have been deliberately inclined in order to produce inside/outside contrast reversal with inversion of the diffraction vector. The large defect structure at the top of the micrographs is included to confirm the same area has been maintained. Scale markers in (a) and (c) apply to (b) and (d–h), respectively.
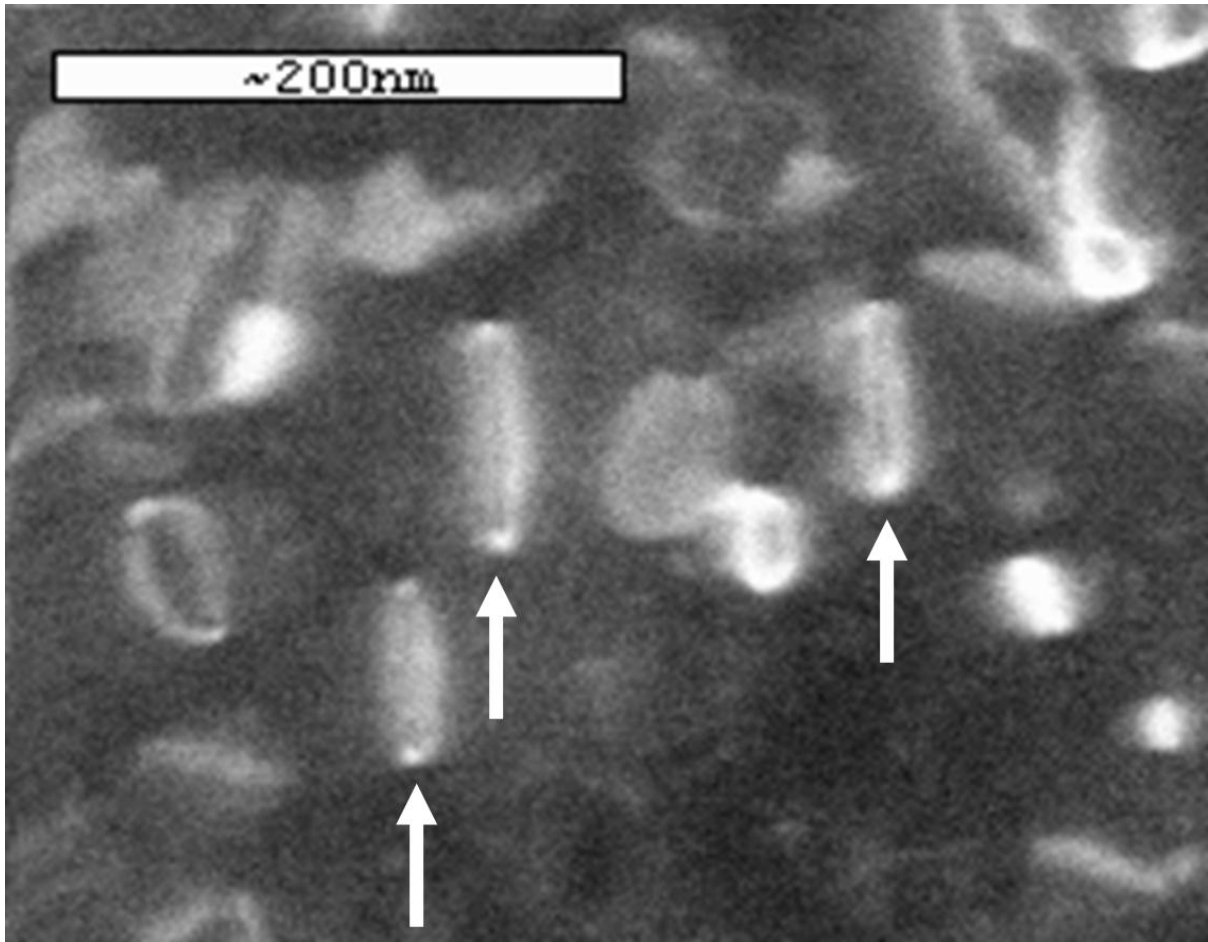
Figure 8: Annular dark-field TEM micrograph of {112}-type dislocation loops, in a close to edge-on orientation, indicated with white arrows (image courtesy of R. Brydson, University of Leeds, United Kingdom).
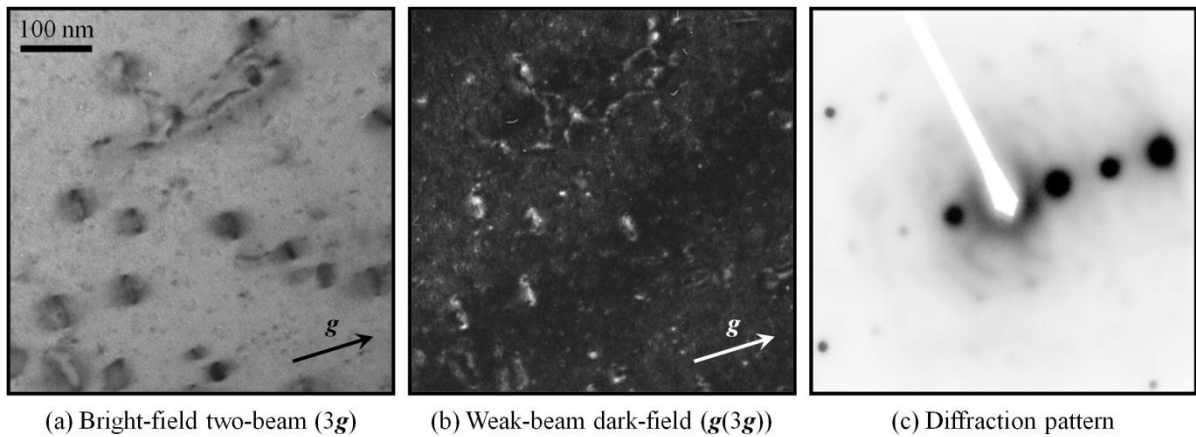
(a) Bright-field two-beam (3*g*)   (b) Weak-beam dark-field (*g*(3*g*))   (c) Diffraction pattern

Figure 9: Underfocus TEM micrographs with g = $1\bar{1}\bar{2}$ ($s_g > 0$) and corresponding diffraction pattern. Scale marker applies to both micrographs.
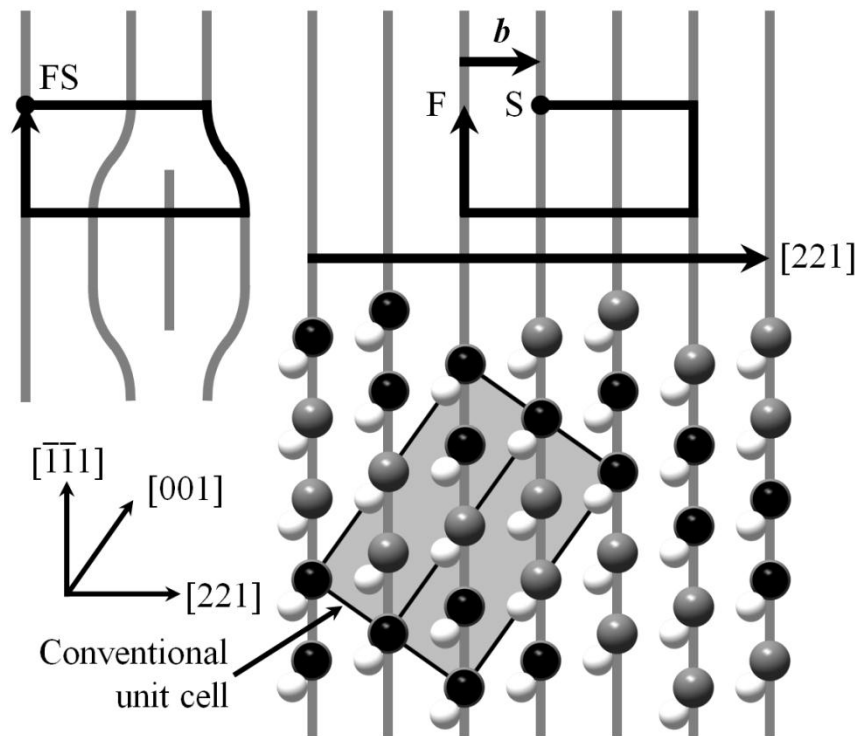

Figure 10: Determination of the Burgers vector using the Finish-Start/Right-Hand (FS/RH) convention looking at (112) planes down the [$1\bar{1}0$] direction. In the FS/RH convention, the Burgers vector is determined by forming a closed circuit around the dislocation (from finish to start) in a clockwise direction (right hand). The dislocation is then removed to leave a perfect crystal and the Burgers vector is the vector required to close the circuit. As shown here, the Burgers vector for the dislocation loops in CIS on {112} planes is b = 1/6 <221>. (Diagrammatic depiction of FS/RH convention after [79].)
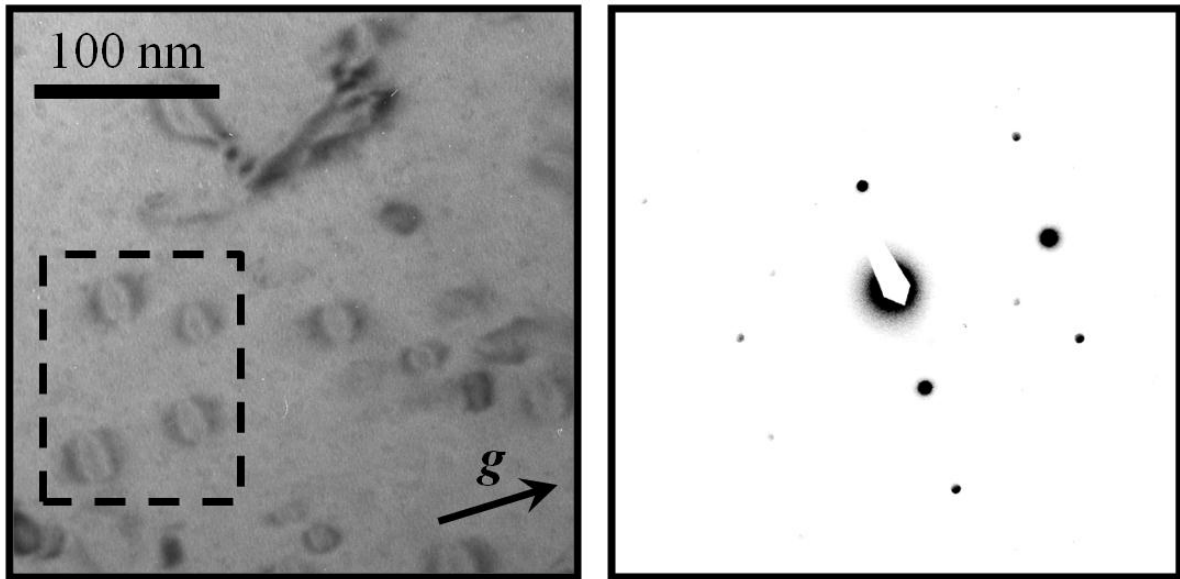
(a) $\boldsymbol{g} = 1\overline{3}\overline{6}$
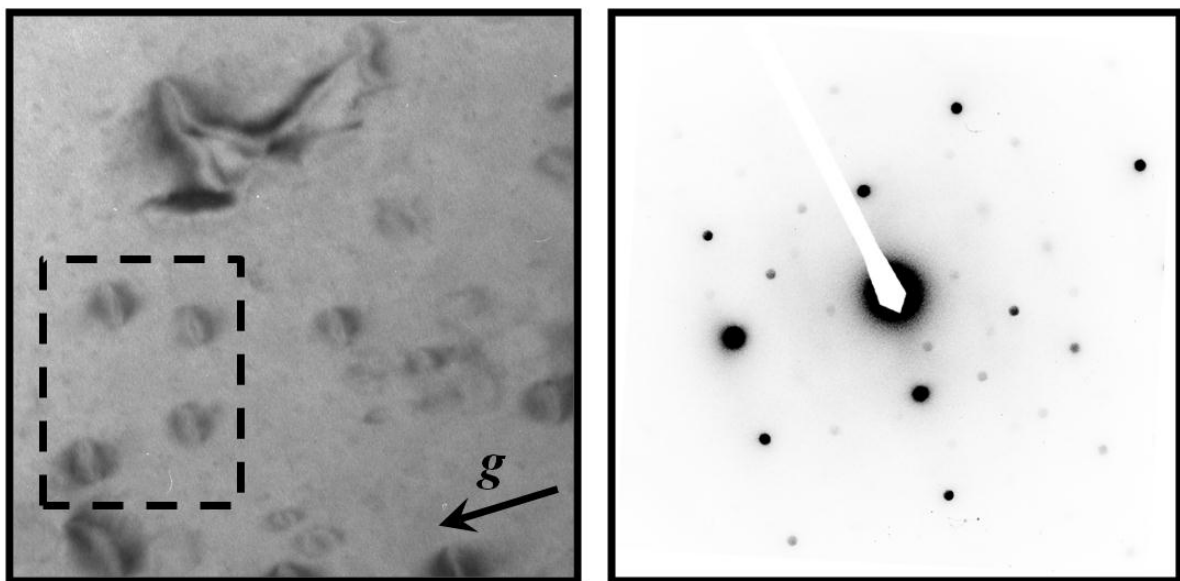
(b) $\boldsymbol{g} = \overline{1}36$

Figure 11: Underfocus bright-field two-beam TEM micrographs ($s_g > 0$) showing determination of dislocation loop nature using the inside/outside contrast technique. Dashed rectangles highlight four examples of inside/outside contrast reversal for the same dislocation loops highlighted and identified as {112}-type in Figure 7 – however, other instances of equivalent inside/outside contrast reversal are also evident in these micrographs. Scale marker applies to both micrographs.
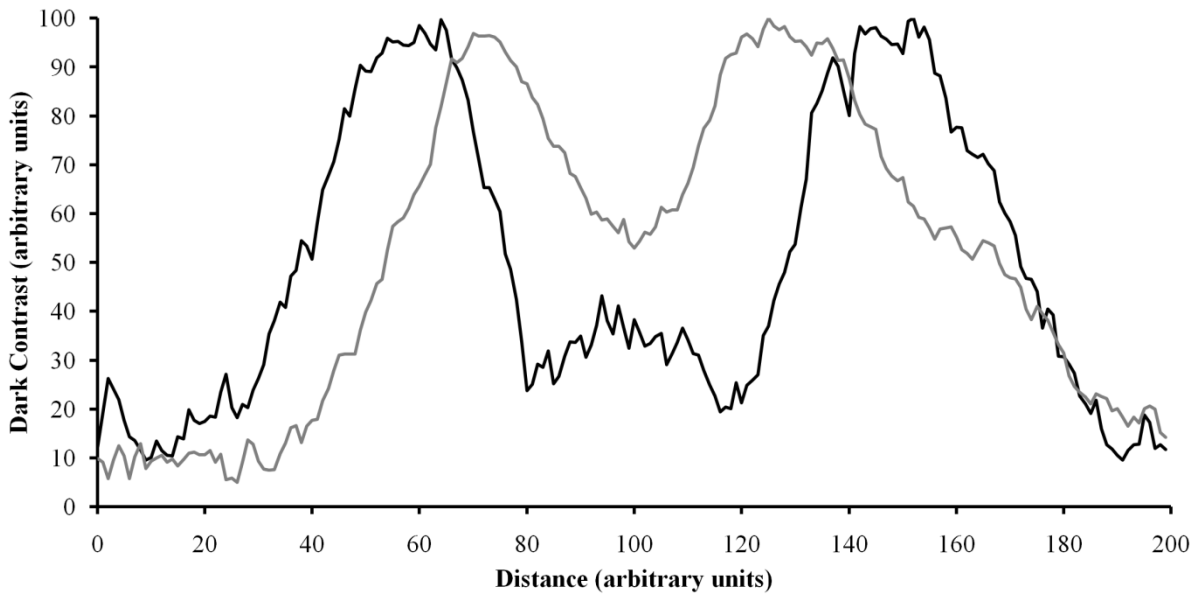
Figure 12: Linescan of contrast against distance across a dislocation loop shown in Figure 11 confirming change in position of contrast due to reversal of direction of diffraction vector from g = $1\overline{3}\overline{6}$ (—) to g = $\overline{1}36$ (—).

Electron beam

$g_{1\overline{3}\overline{6}}$ $g_{\overline{1}36}$

Position of diffraction contrast (———)
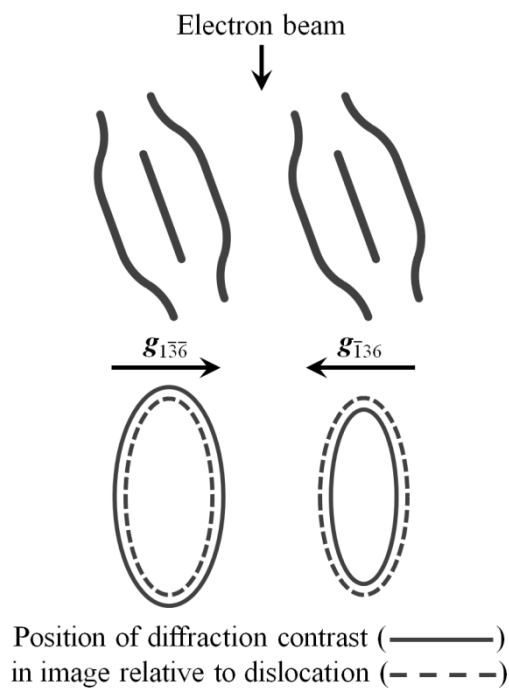in image relative to dislocation (– – – –)

Figure 13: Schematic diagram illustrating the combinations of dislocation loop inclination, nature and diffraction vectors for a positive value of the deviation parameter ($s_g > 0$) which lead to the switching of the location of the diffraction contrast between the inside and outside of the dislocation in Figure 11.
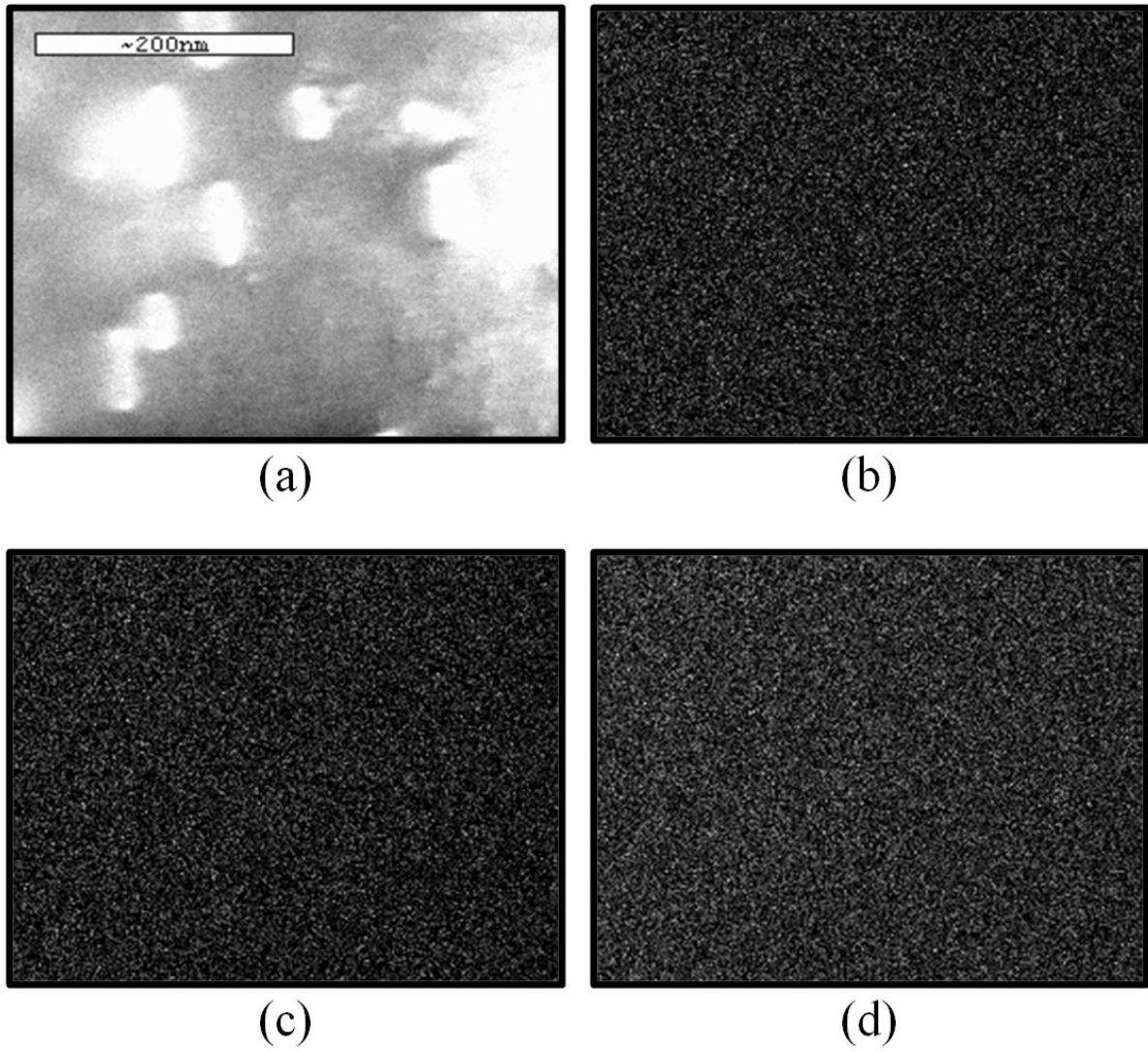
Figure 14: STEM EDS results for a region containing end-on interstitial dislocation loops showing (a) an ADF image and corresponding maps for the (b) copper, (c) indium and (d) selenium signals (courtesy of R. Brydson).